

Article

Spread Spectrum Induced Polarization (SSIP) Survey for the Qiushuwan Copper–Molybdenum Deposits in Southern Henan Province, China

Jawad Ahmad ^{1,2} , Rujun Chen ^{1,2,*} , Ijaz Ahmed ^{1,2}, Muhammad Yaseen ^{1,2,3} , Shahid Ali Shah ^{1,2}, Osama Abdul Rahim ^{1,2}, Farid Ullah ^{1,2}, Shah Fahad ^{1,2} and Li Rui ^{1,2}

¹ School of Geosciences and Info-Physics, Central South University, Changsha 410083, China; jawadahmad_9090@csu.edu.cn (J.A.); 215018004@csu.edu.cn (I.A.); yaseengeo@awkum.edu.pk (M.Y.); 225018006@csu.edu.cn (S.A.S.); 205018013@csu.edu.cn (O.A.R.); faridullah@csu.edu.cn (F.U.); 215018017@csu.edu.cn (S.F.); frankinglee@163.com (L.R.)

² AIoT Innovation and Entrepreneurship Education Center for Geology and Geophysics, Central South University, Changsha 410083, China

³ Faculty of Physical and Numerical Sciences, Department of Geology, Abdul Wali Khan University, Mardan 23200, Pakistan

* Correspondence: chrujun@csu.edu.cn

Abstract: The Qiushuwan Cu-Mo deposit, situated in the East Qinling molybdenum belt, is a notable mining site renowned for its considerable quantities of medium-sized molybdenum. The goal of this study is to improve comprehension and identify additional mineral resources by conducting a thorough examination of the mine using the spread spectrum-induced polarization (SSIP) technique. Gathering SSIP data, conducting geological investigations, and examining the electrical characteristics of rock and mineral samples along Profile-80 led to significant discoveries. The investigation identified two significant ore bodies with high conductivity: C2, linked to granite porphyry and molybdenum veins, and C4, associated with a skarn deposit containing a concentrated amount of copper ore. This study used resistivity models created from SSIP data to find out how conductivity changed in different parts of the research area. Additional drill verifications validated these findings, indicating the presence of potential mineral resources. The petrographic analysis of core samples showed that minerals like pyrite, molybdenite, chalcopyrite, epidote, calcite, and garnet were present. Notably, the samples frequently contained both pyrite and molybdenite together. Sample 04-2 contained substantial quantities of molybdenite and pyrite; Sample 05-1 had occasional pyrite; and Sample 07-4 included both pyrite and chalcopyrite. These findings offer useful insights for evaluating the magnitude and economic feasibility of the mineral deposits; however, additional investigation is required to completely comprehend the scope of the resources. The integration of borehole data and the alignment of geological sections with inversion models confirmed the validity of the conclusions. The core samples that were retrieved show a lot of different minerals, including valuable ores and minerals that have been changed. Pyrite and molybdenite are always found together. These findings establish a solid basis for further investigation and the sustainable management of resources. This study contributes to the understanding of the Qiushuwan Cu-Mo deposit and advances exploration techniques using the spread spectrum-induced polarization (SSIP) method. It provides useful information for geologists, mining professionals, and stakeholders involved in resource usage.



Citation: Ahmad, J.; Chen, R.; Ahmed, I.; Yaseen, M.; Shah, S.A.; Rahim, O.A.; Ullah, F.; Fahad, S.; Rui, L. Spread Spectrum Induced Polarization (SSIP) Survey for the Qiushuwan Copper–Molybdenum Deposits in Southern Henan Province, China. *Minerals* **2024**, *14*, 934. <https://doi.org/10.3390/min14090934>

Academic Editor: Michael S. Zhdanov

Received: 8 August 2024

Revised: 5 September 2024

Accepted: 7 September 2024

Published: 13 September 2024

Corrected: 9 June 2025



Copyright: © 2024 by the authors. Licensee MDPI, Basel, Switzerland. This article is an open access article distributed under the terms and conditions of the Creative Commons Attribution (CC BY) license (<https://creativecommons.org/licenses/by/4.0/>).

Keywords: copper–molybdenum deposits; spread spectrum-induced polarization; mineral resources; Qiushuwan deposits; geophysical method

1. Introduction

Thorough research and development in multiple mining regions are crucial in the mining sector, given the increasing demand for natural resources in China. China is a

prominent producer and distributor of copper and molybdenum, with substantial reserves all over the country [1]. The Qiushawan Cu-Mo deposit, situated in the Shangdan fault zone of Henan Province, is a significant copper–molybdenum deposit known for its porphyry-skarn mineralization. Although China possesses abundant confirmed reserves, the quality of copper and molybdenum ores is often inferior to that of major resource countries such as the United States and Chile. The majority of China's reserves are classified as low-grade [2]. Henan Province possesses the most extensive molybdenum reserves in China, with 30.1% of the country's overall stockpile. Currently, there is ongoing investigation and development of the Qiushawan deposit, which uncovers favorable geological characteristics indicating the presence of substantial copper and molybdenum mineral deposits [3]. The deposit, which was formed during the late Mesozoic granitic magmatism in the North Qinling region, is located about 15 km north of Zhenping town. It contains around 98 kilotonnes of copper with an average grade of 0.72% and 1.66 kilotonnes of molybdenum with a grade of 0.12% [4]. From a geological perspective, it is located in the eastern section of the Eastern Qinling Orogenic Belt, approximately 10 km to the north of the Shangdan Fault. This fault acts as a boundary between the North and South Qinling regions [5]. Since the 1970s, the Qiushawan Copper Molybdenum Mine has continuously conducted exploratory activities. The deposit shares notable similarities with other substantial deposits in the East Qinling Copper–Molybdenum Mine Belt [6]. In order to improve exploration in the Qiushawan area, the study utilizes the spread spectrum induced polarization (SSIP) geophysical exploration technique for the purpose of exploring copper and molybdenum ore [7].

2. Regional Geology

The Qinling–Dabie Orogenic Belt, located in the eastern part of Central China, is one of the economically significant collisional orogens in eastern Asia. This orogenic belt marks the suture zone between the North China Craton (NCC) and the Yangtze Craton (YC) and is broadly subdivided into two units: the North Qinling and the South Qinling, which are separated by the Shangdan Suture Zone (Figure 1). In the early Paleozoic, the NCC and the YC were separated by the Paleo-Tethys Ocean. The middle Paleozoic collision along the Shangdan Suture Zone accreted the South Qinling terrane to the southern part of the North China Craton (i.e., the North Qinling terrane). Subsequent middle to late Paleozoic rifting and drifting separated the South Qinling terrane from the YC [8]. The Triassic collision of the YC with the South Qinling terrane led to the final integration of the orogenic belt. The Early Mesozoic continent-continent collision between the YC and NCC resulted in an over-thickened continental crust, followed by uplift and extensional tectonic collapse from the Middle Jurassic to the Early Cretaceous. The rock units in the Qinling–Dabie Orogenic Belt have complex lithologic associations. The North Qinling terrane is dominantly composed of middle Paleozoic medium-grade metasedimentary and metavolcanic rocks. The basement of this terrane mainly consists of the Mesoproterozoic Qinling Group, which includes biotite plagioclase gneiss, granulite, amphibolite, dolomitic, and graphitic marbles. The Neoproterozoic Kuanping Group consists of meta-basalts, clastic, and carbonate rocks. In contrast, the South Qinling terrane consists of meta-volcanic rocks and meta-sedimentary rocks (Neoarchean Yudongzi Group), amphibolite, leptite, migmatite, the Douling gneiss-amphibolite marble, and Neoproterozoic volcanic rocks, as well as overlying Cambrian to Triassic sedimentary rocks. Additionally, late Mesozoic (Late Jurassic to Middle Cretaceous, the so-called “Yanshanian” in Chinese literature) granitoids are also widespread in the Qinling–Dabie orogenic belt and commonly intruded the Archean to Neoproterozoic metamorphic rocks in the orogenic belt (Figure 1). The porphyry and skarn Mo deposits are spatially and temporally associated with the granitic rocks that mainly outcrop across the Launchman fault in the orogeny.

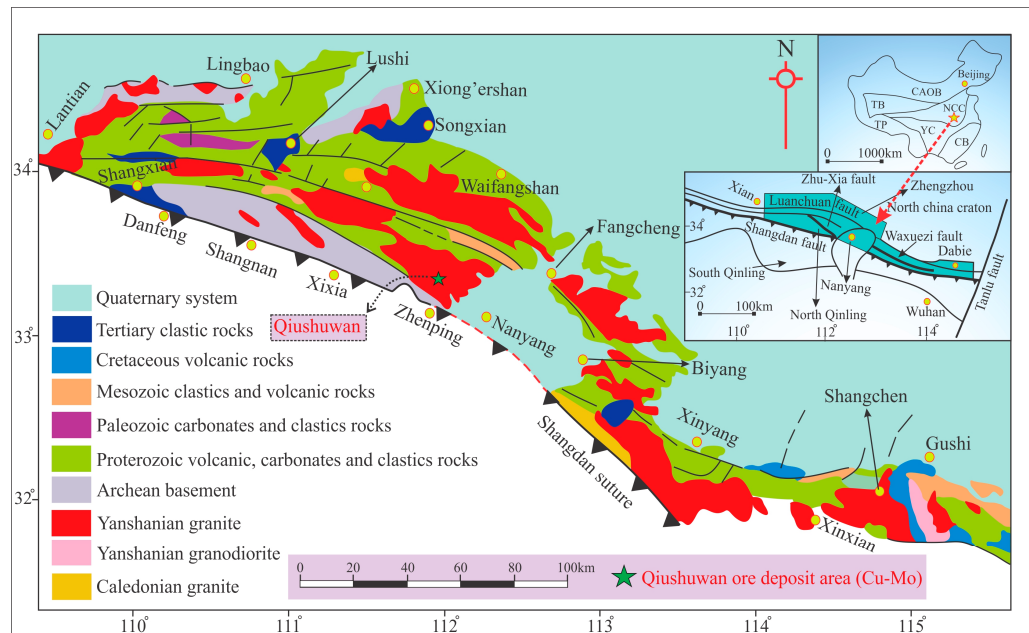


Figure 1. Geological map of the study area. Significant abbreviations used in the regional China map include CB (Cathaysia Block), YC (Yangtze Craton), NCC (North China Craton), TP (Tibetan Plateau), TB (Tarim Block), and CAOB (Central Asian Orogenic Belt). This map serves as a valuable visual aid for understanding the geological context of Mo ore deposits in the Qinling–Dabie Orogenic Belt, modified after Liu et al. (2021) [9].

3. Deposit Geology

The Cu-Mo deposit of Qiushuwan is situated in the northern region of the Shangdan Suture Zone, precisely within the North Qinling terrane [10]. The region is distinguished by a structural framework comprising NWW and NW-oriented structures, which align with the area's tectonic lineaments [9]. The Early Proterozoic Qinling Group is the primary rock formation in the region, characterized by schist, marble, and granitic gneiss [11]. The sedimentary accumulation is linked to Mesozoic quartz porphyries and porphyritic granodiorites, which constitute the majority of the granitoids (Figure 2). Quartz porphyries are observed to penetrate the Early Proterozoic Qinling Group through faults trending in either a northeastern or westerly direction. These porphyries manifest as irregular-shaped stocks or dikes on the surface [12]. The formation of NWW-trending bodies within a synclinal core is closely associated with porphyritic granodiorite, which is directly tied to Cu-Mo mineralization [13]. The region where the porphyritic granodiorites come into contact with the adjacent wall rock displays significant alterations, such as skarnization, silicification, potassic alteration, sericitization, and pyritization [14]. In the Qiushuwan porphyry-skarn Mo deposit, the predominant ore minerals consist of molybdenite and chalcopyrite, with chalcopyrite found as dispersed crystals and locally polymerized forms [15]. The area is located in the northern region of Zhenping County, Henan Province, within the eastern portion of the North Qinling tectonic subzone, which is part of the broader Qinling orogenic belt [16]. The visible rock formations in the area are classified as part of the Qinling Group. There is a structural connection between the Yanlinggou Formation, primarily composed of carbonate, and the Guozhuang Formation, primarily composed of granite gneiss [17]. The major orientation of the area's fault system is northwest-southeast, corresponding to the Zhuxia Fault that traverses the Qinling Group strata (Figure 2) [18]. The deposit comprises two primary constituents: the northern section, distinguished by a copper-molybdenum deposit of breccia type found within the explosive breccia, and the southern section, characterized by a molybdenum deposit of porphyry-skarn type within the Qiushuwan granodiorite porphyry and its adjacent contact zone [19]. The mineralization displays clear zoning patterns, with molybdenum mineralization predominantly in the

southwestern zone, while copper mineralization is more commonly observed in the north-eastern section. This zoning pattern indicates the presence of molybdenum mineralization superimposed upon pre-existing copper mineralization [20].

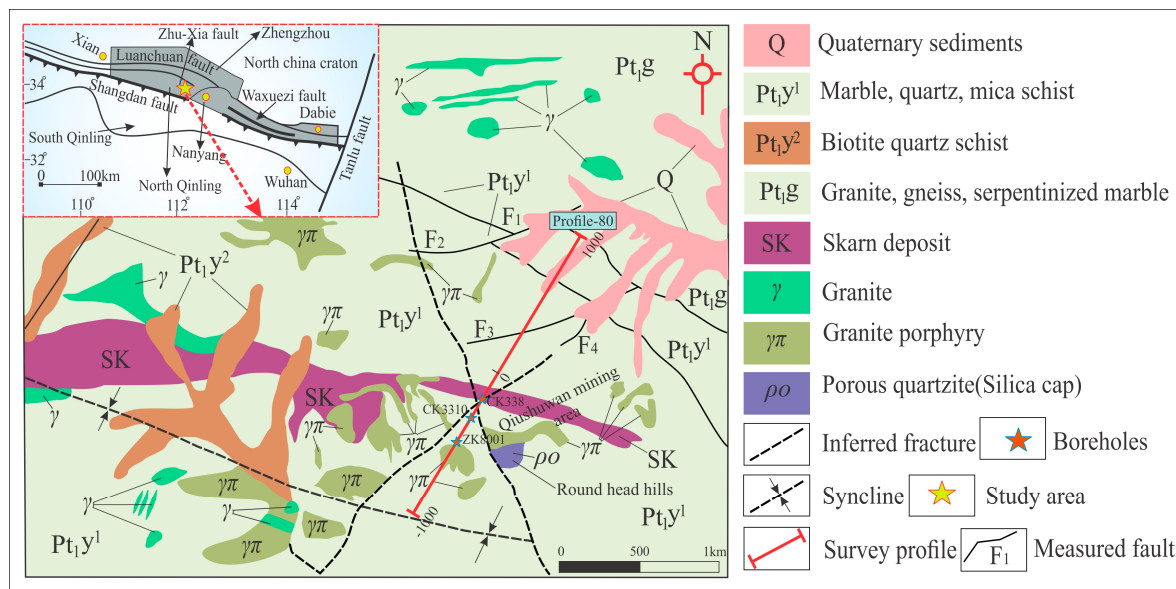


Figure 2. The geological map of the Qiushuwan Cu–Mo deposit along with the survey profile as mentioned, L-80.

4. Electrical Parameters and Data Analysis

Geological samples were collected from the Qiushuwan mining area in Henan Province, and some of these samples were tested for effective rock and ore electrical characteristics parameters (Table 1). The lithology includes marble, granodiorite, plagioclase hornblende, chlorite siliceous rock, garnet siliceous rock, quartzite, explosive breccia, and ore-bearing quartz veins. The main types of mineralization include pyrite mineralization, molybdenization, and brass mineralization. The primary alterations observed are carbonatization, chloritization, epidotization, and skarnization. According to the statistical data of electrical parameters of Qiushuwan rock (ore) in Table 1, the electrical resistivity (ρ_s) and chargeability (η) of the collected samples vary significantly. Epidote and chloritized skarn show low resistance and high chargeability anomalies compared to other lithologies and rock electrical characteristics. These observations indicate that the mineralization of pyrite, chalcopyrite, and molybdenite in this mining area is closely related to chlorite and epidotized skarn, suggesting strong mineralization of pyrite and molybdenite in the rock (ore) of this lithology. Additionally, the resistivity and chargeability values of garnet and garnet skarn vary significantly. Garnet that have not undergone mineralization or are relatively weakly mineralized often contains silicification alteration, resulting in a higher resistivity ranging from 1037 to 19,823 $\Omega\cdot m$. In contrast, garnet skarn that has undergone mineralization has a relatively lower resistivity, with an average resistivity of 3.074 $\Omega\cdot m$, and an average chargeability of 2.16%. However, due to the lower mineralization intensity compared to chlorite and epidote skarn, the electrical anomaly is not significant (Figure 6b). At the same time, marble, granodiorite, and quartzite (veins) all exhibit high resistivity and low chargeability anomalies. Metal minerals in these rocks are mostly sparsely disseminated, with weak mineralization intensity. Biotite plagioclase hornblende and plagioclase hornblende undergo varying degrees of chloritization, and some contain explosive breccia (mineralization). Their resistivity and chargeability values are intermediate between rocks with strong low-resistance mineralization, such as chlorite and epidote skarn, and high-resistance marble.

Table 1. Ore electrical characteristics parameters in the study area.

| Rock-Ore Specimen | Resistivity ρ ($\Omega \cdot \text{m}$) | Chargeability η (%) |
|---|--|--------------------------|
| | Range of Variation | Range of Variation |
| Marble | 3548 ± 9~69,236 ± 7 | 0.07~2.68 |
| Biotite plagioclase hornblende | 242 ± 5~3686 ± 8 | 0.27~0.96 |
| Granodiorite | 7550~38,103 | 0.59~3.05 |
| Quartz and epidote skarn interbedding | 687 ± 3~15,381 ± 2 | 0.76~4.57 |
| Petrified skarn | 4.77~13,016 ± 5 | 0.24~13.43 |
| Contact zone between garnet and epidote skarn | 2110 ± 4~8218 ± 10 | 2.64~9.49 |
| Garnet skarn | 5.90~14,404 ± 5 | 0.21~1.08 |
| Ore-bearing quartzite (vein) | 1392 ± 1~34,473 ± 9 | 0.38~8.62 |
| Plagioclase hornblende | 556 ± 9~1971 ± 2 | 0.44~2.66 |

5. Methodology

The spread spectrum-induced polarization (SSIP) method is a new frequency domain-induced polarization (FDIP) method. It uses spread spectrum communication for geophysical instruments [21]. This system boasts characteristics such as greater depth penetration, high precision, resistance to anti-interference, cost-effectiveness, and efficiency. The identification approach has garnered more attention and development due to its highly effective denoising capability. It is currently widely adopted and has delivered significant social and economic benefits. The primary difference between FDIP and SSIP methods lies in the type of signal used for the injected (primary) current. The SSIP system transmits M-sequence pseudo-random spread spectrum signals via the transmitter as the primary current source. In traditional FDIP, rectangular current waves with constant duration intervals are typically used [22].

In SSIP surveys, a comparison is made between the voltage signals measured at potential electrodes and signals transmitted through the current electrodes across multiple frequencies (i.e., a spectrum of frequencies). The frequency band of SSIP acquisition is 1/16 to -1 Hz , and the amplitude of the primary injected current depends on the strength of electromagnetic EM interferences in the surveyed area. Specifically, in areas with intense (EM) interferences from activities such as mining operations and drilling, larger primary current amplitudes are used. The apparent complex resistivity for a range of frequencies can be obtained similarly to traditional FDIP approaches:

$$\rho(f) = K \frac{U(f)}{I(f)} \quad (1)$$

where $\rho(f)$ stands for the apparent resistivity, $U(f)$ denotes the frequency spectrum of the potential difference data, $I(f)$ is the frequency spectrum of synchronous primary current data, and K corresponds to the geometric factor of the array.

$$\frac{1}{K} = \frac{1}{2\pi} \left[\left(\frac{1}{AM} - \frac{1}{BM} \right) - \left(\frac{1}{AN} - \frac{1}{BN} \right) \right] \quad (2)$$

Here, A and B are current electrodes, and M and N are potential electrodes. AM , BM , AN , and BN are electrode spaces.

Data Acquisition

The SSIP approach operates using multi-channel equipment to observe arrays in parallel. By utilizing GPS synchronization technology between transmitter and receiver, this method streamlines the electrode arrangement process of the electrical sounding profile and enables simultaneous multiple measurements. This reduces the need for repeated transmission from the power supply electrode, thereby increasing measurement speed. In regions characterized by dry and high resistance, the reduced mobility of the power supply electrode improves grounding conditions, allowing for increased power supply

current. This enhancement in observation accuracy occurs progressively, starting with small increments and increasing towards the center of the measuring line. Power is first supplied to $(-10\text{ m}, 10\text{ m})$, $(-50\text{ m}, 50\text{ m})$, followed by $(-1010\text{ m}, 1010\text{ m})$, and so forth. In industrial settings with significant electrical interference, such as mines, it is advisable to prioritize the placement of electrodes and cables. We conducted a 2 km SSIP survey profile near the Qiushuwān mining region, located between the Yanlinggou and Guozhuang formations, in a SW-NE direction (Figure 2). The receiving electrodes for the whole profile were successfully installed in a single operation. The construction approach employed for this project involved measuring the depth of the nonconventional gradient array using spread spectrum-induced polarization. The number of measurement points depends on the dimensions of the profile, specifically its length and space. Subsequently, measurement electrodes and data collection stations are implemented simultaneously across the entire profile. Electricity is then distributed sequentially according to predetermined current injection sites using brass electrodes. All channels are monitored simultaneously during each current injection. Once all designated power supply sites have been completed, the comprehensive profile measurement is concluded. Set of SSIP equipment and array used is shown in Figure 3 and Figure 4, respectively.

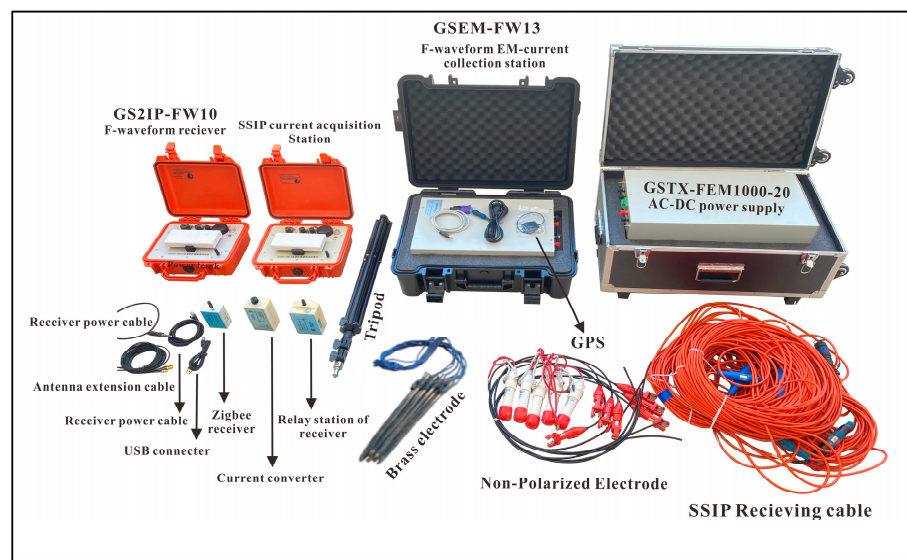


Figure 3. Set of equipment used during SSIP exploration survey (modified from GSAI) [23].

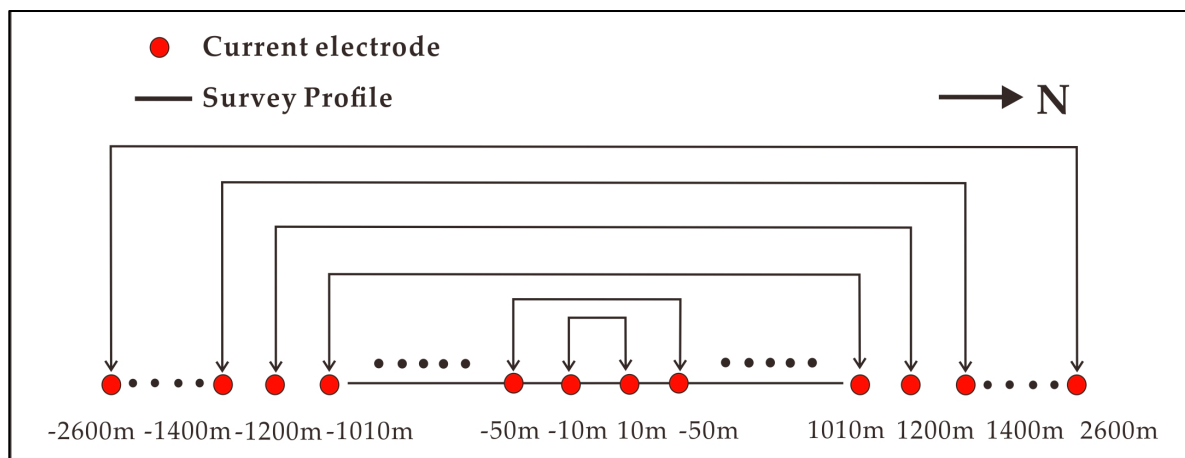


Figure 4. The nonconventional gradient array protocol for the SSIP survey profile, utilizing 34 current electrodes with a maximum spacing of 5200 m and a minimum spacing of 20 m. The 2000 m line features potential electrodes spaced 20 m apart, modified based on Liu et al. (2017) [21].

6. Results and Discussion

6.1. Inversion Parameters

The precision of our SSIP results was paramount; therefore, we meticulously selected key parameters in ZondRes2D and implemented complex procedures (Figure 5). The choice of these metrics was deliberate to ensure the accuracy and reliability of our findings. The inversion setup began with a 5 m thick initial layer, with model parameters systematically adjusted in subsequent iterations using an incremental factor of 1.10%.

The inversion process comprised 32 layers, reaching a maximum depth of 1005 m. Additionally, we applied standard model constraints by setting values ranging from $1.0 \Omega \cdot \text{m}$ to $10,000 \Omega \cdot \text{m}$, establishing minimum and maximum limits. The resistivity data exhibited a fitting error of 4.8%, while the relative phase data (chargeability data) indicated a fitting error of 2.1%.

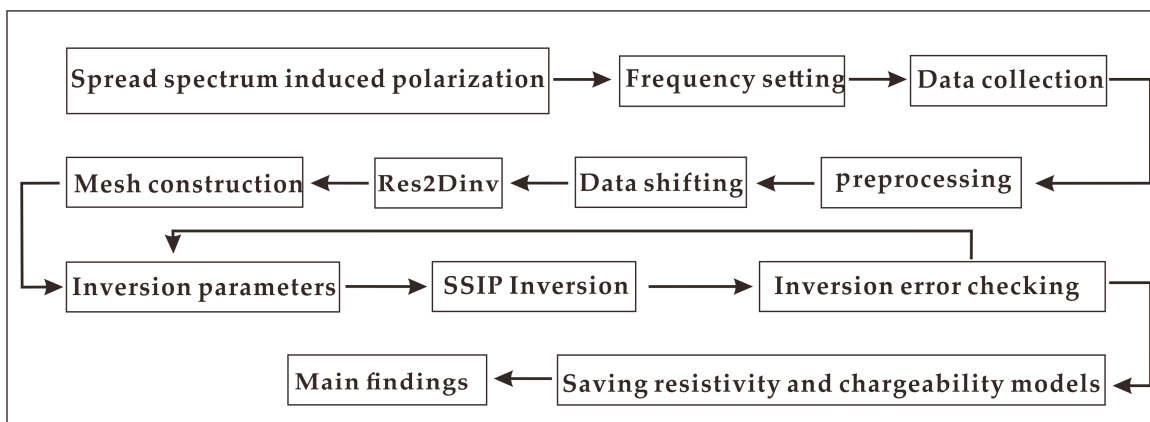


Figure 5. Showing the overall data collection and inversion parameter steps for the resistivity and chargeability model of SSIP.

6.2. Inversion Results

The Profile-80 (NE-SW) is located in the eastern part of the exploration area (Figure 2). The inversion results of one kilometer of the original profile (2 km) are shown in Figure 6. The resistivity models derived from the SSIP frequencies show no significant differences, with the example of the best results obtained at frequency F2 (0.203125). The data from Profile-80, collected over the Qiushawan Cu-Mo deposit, exhibit distinct characteristics marked by spatial variations in electrical resistivity. The resistivity model, as illustrated in Figure 6, identifies four conductive regions (C1, C2, C3, and C4) with moderate to high conductivity and four regions with moderate to high resistivity (R1, R2, R3, and R4). The conductive zones are characterized by a resistivity of less than $1800 \Omega \cdot \text{m}$. Resistivity variation is high in SW and low in the NE of the one-kilometer inversion, as shown in Figure 6a. In the SW, resistivity ranges from 2800 to 3000 $\Omega \cdot \text{m}$, with vertical anomalies appearing high in the shallow section and low in the deeper part. In the shallow southwest (SW) section, we encounter the C1 conductive body (surficial material) from the surface to a depth of 290 m, spanning horizontally from -1000 to -900 m. Notably, feature R1 (marble, quartz, mica, schist) presents a horizontally extensive high resistivity anomaly between depths of -880 and -1000 m. This anomaly reaches a maximum resistivity value exceeding $3500 \Omega \cdot \text{m}$ and is centered at an elevation of approximately 370 m. In the middle of the resistivity model, R2 (same lithology as R1) is observed at shallow depths of 290 to 190 m, confined horizontally between -700 and -600 m. Moving to the central section of the inversion model, another distinct anomaly, C2 (granite porphyry with molybdenum veins), appears between depths of -830 and -570 . This anomaly exhibits a moderate to high resistivity with a maximum exceeding $3000 \Omega \cdot \text{m}$ and shows a longitudinal extension trend. In the northeast (NE), resistivity values vary from high to low; additionally, a moderate resistivity anomaly, R3 (granite, gneiss, and quartz), is identified between depths of -160

and -370 m, with a maximum value below $3000 \Omega \cdot \text{m}$. This anomaly shows a downward continuation pattern. Near the surface, the C3 conductive body and R4 resistive body are located close to each other. The large conductive body C4 (skarn deposits) is situated from an elevation of -50 m to the exploration depth, spanning horizontally from -150 to around 0 m.

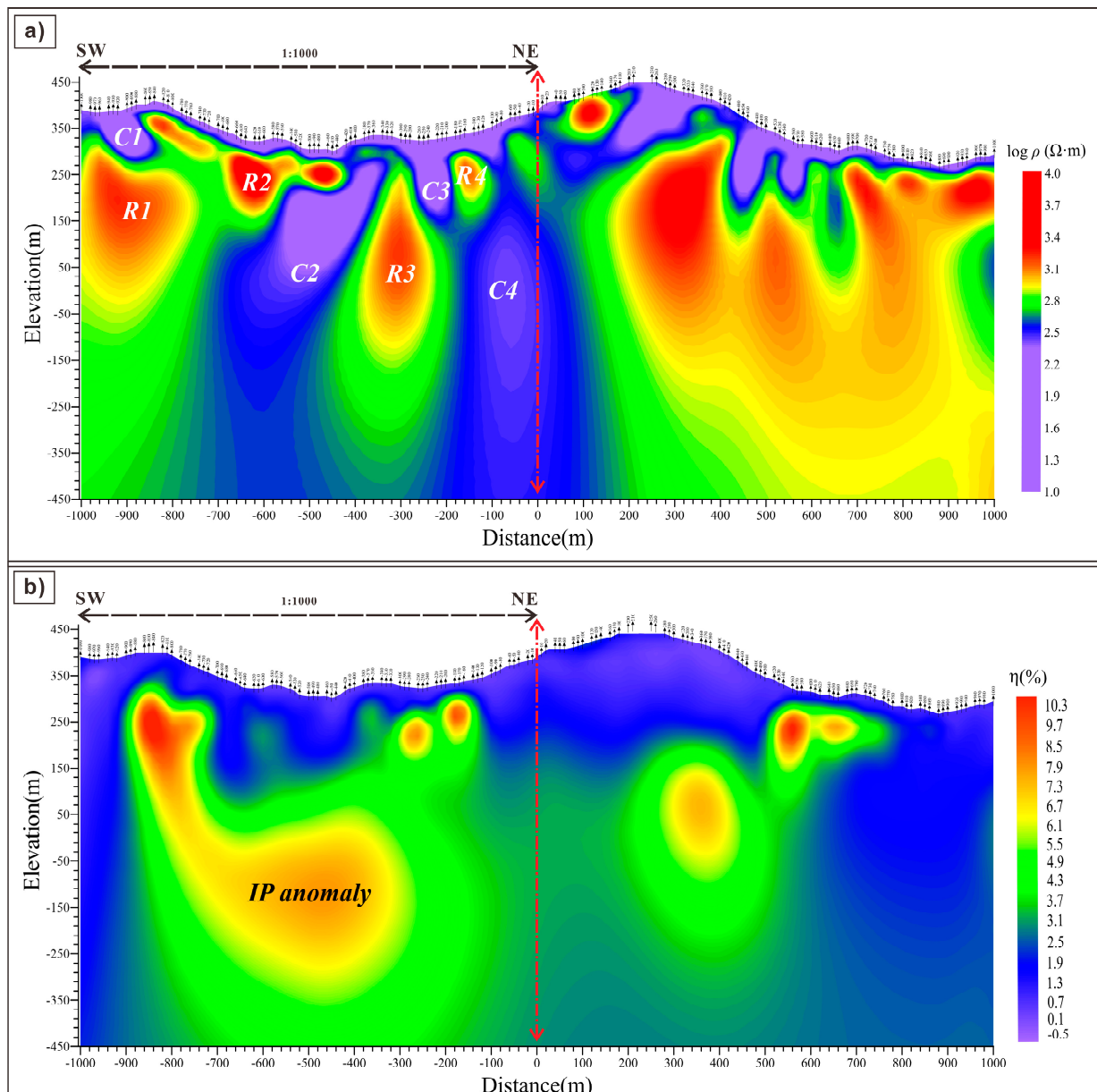


Figure 6. SSIP inversion results of L-80: (a) the resistivity model of L-80 showing the interpreted subsurface structure and lithological unit, and (b) the chargeability model of L-80 showing IP anomalies and zones of mineralization.

Figure 6b shows the IP inversion model where the IP anomaly is centered and extended towards the northeast.

By utilizing the appropriate F2 frequency, the analysis of SSIP data, combined with geological information from the study area, provides valuable insights into the properties of conducting bodies C2 and C4. This study includes an analysis of the electrical properties of rock and ore specimens, with a specific focus on resistivity values (Table 1). This analysis also includes the examination of geological sections, 2D resistivity models, and IP inversion models (Figure 7).

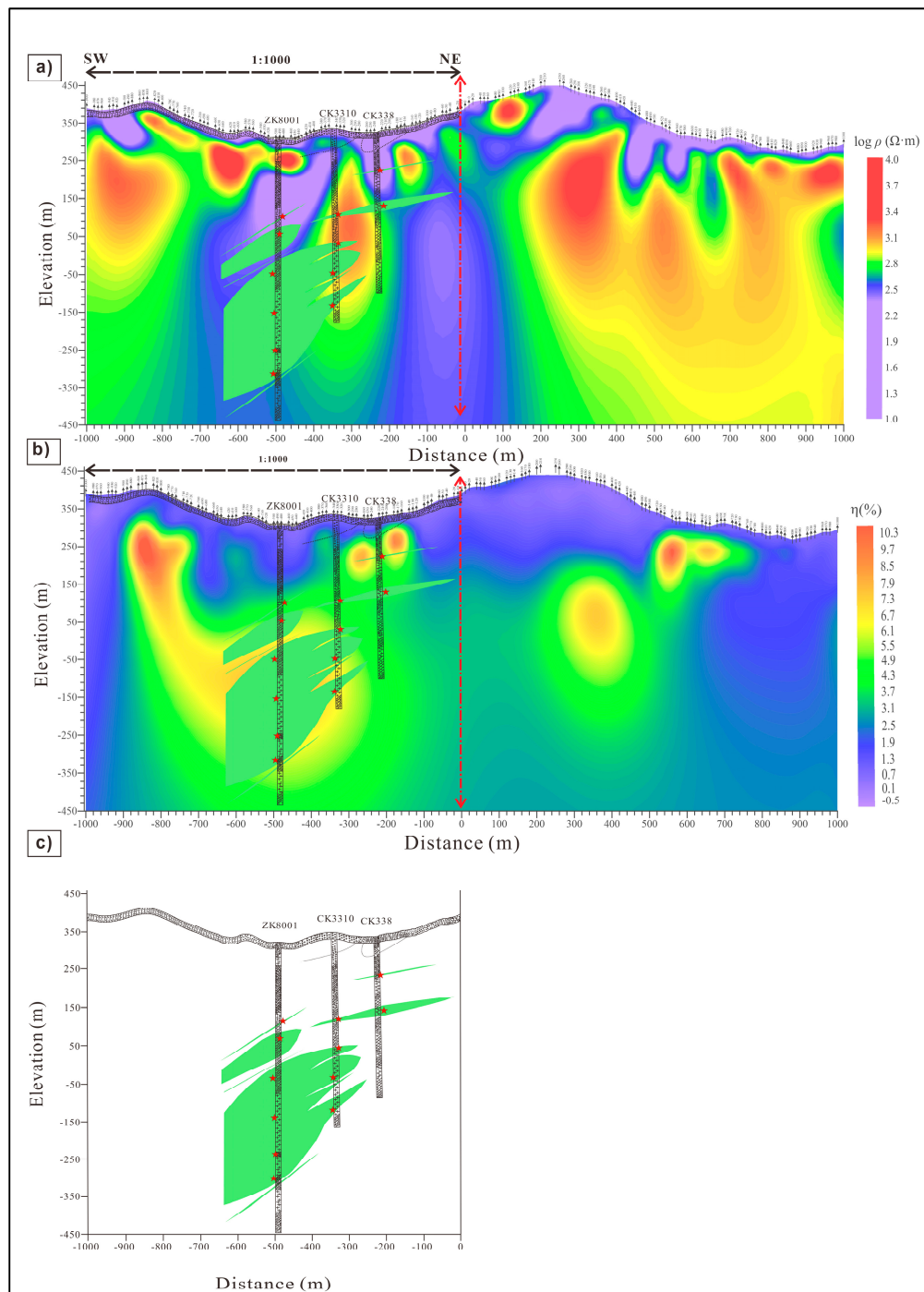


Figure 7. Displaying 2D resistivity IP inversion slices (a,b) overlaps with the geological model (c), showing the location and trend of ore bodies.

The inversion results revealed the presence of two primary conducting bodies, C2 and C4, within the designated region. Analysis of the data concluded that conductive body C2 is associated with granite porphyry hosting molybdenum veins (Figure 8). The resistivity values obtained from rock and ore samples within this formation correspond to the conductive pattern observed in the SSIP data, indicating that the presence of molybdenum veins influences the conductivity of the granite porphyry. In contrast, conductive body C4 is linked to a skarn deposit containing breccia tuff, within which a copper ore body is present. The geological section aligns with the 2D resistivity model and the IP inversion model, confirming the presence of conducting bodies C2 and C4 in this area. The presence

of breccia tuff supports the association between conductive body C4 and the skarn deposit. The copper ore body within the skarn deposit represents a highly prospective target for potential mining operations.

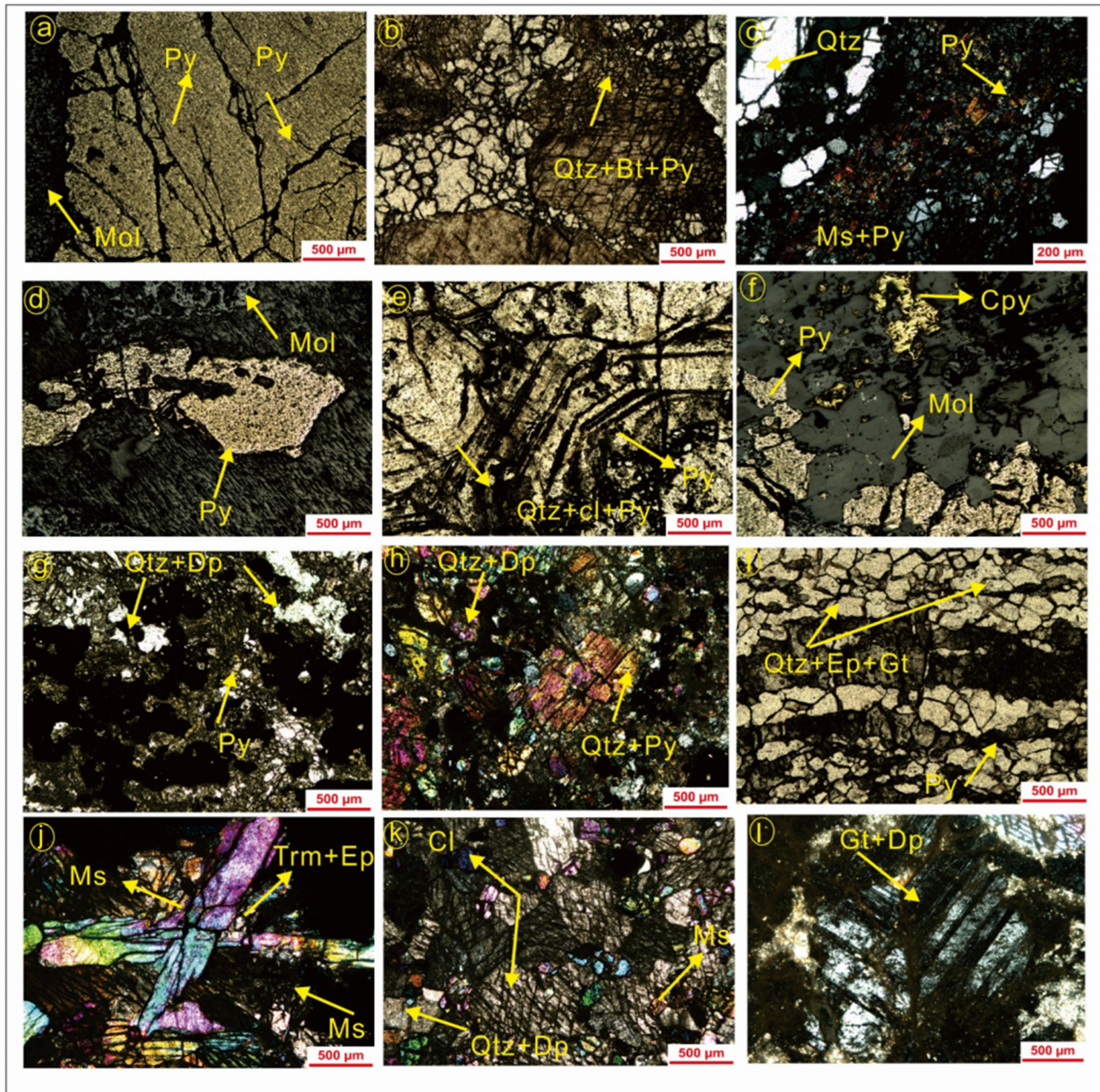


Figure 8. (a) Sample (04-2): Consisting entirely of massive pyrite (Py) and molybdenite (Mol) associated with skarns. (b,c) Sample (05-1): Displaying pyrite (Py) sparsely disseminated in skarn with a small amount of biotite (Bt) and quartz (Qtz) generated along the cracks. (c): Sample (05-1) muscovite (Ms) and biotite (Bt) in quartz and feldspars with pyrite (Py). (d,e) Sample (05-18): (d) Containing Py and Mol. (e) Visible quartz (qtz), diopside (Dp), and calcite (Cl) with disseminated pyrite (Py). (f) Sample (07-4): Pyrite (Py), chalcopyrite (Cpy) with disseminated possibly galena, sphalerite, or molybdenite (Mol). (g,h) Sample (07-13): Visible disseminated mineralization includes quartz (Qtz), diopside (Dp), and pyrite (Py). (i): Sample (05-21): Quartz (Qtz) and epidote (Ep) skarn interbedded, containing garnet (Gt), with extremely weak mineralization. (j) Sample: (05-6): Contains minerals tremolite (Trm), muscovite (Ms), epidote (Ep), and garnet (Gt). (k) Sample (01-7): Contains muscovite, chlorite, diopside, and calcite. (l) Sample (02-15): Calcium iron garnet, with visible ringed twin crystals and granular diopside.

There is low resistance in the ore body, but there are no ore bodies in multiple low-resistance areas. In these areas, shallow induced polarization weakens, while the induced polarization anomaly caused by the porphyry-type ore body is greatly enhanced. The extent of the anomaly is largely consistent with the range of the ore body. In the medium-frequency induced polarization response, the anomalies of porphyry-type ore bodies are significantly enhanced, whereas the anomalies caused by pyrite halos and skarn-type ore bodies are greatly diminished. This technique is effective in discovering induced polarization anomalies caused by deep porphyry copper–molybdenum deposits.

7. Mineralization and Alteration

Following the SSIP survey, drill verifications such as ZK8001 at point (-470), CK3310 (-330), and CK338 (-220) verified the anomalies and highlighted the presence of probable mineral resources in the study region. The detailed petrography of the drilled core samples revealed a variety of minerals, including ores and some alteration minerals, as shown in Table 2. A total of nine different rock samples were observed under the optical microscope (Figure 8). Pyrite typically occurs with molybdenite in most of the samples. Chalcopyrite, epidote, calcite, and garnet are present as sparse accessory minerals. Figure 6 details all the minerals and their possible alterations. Sample no. 04-2 consists entirely of massive pyrite (Py) and molybdenite (Mol)-associated with skarns. Sample (05-1) displays an association of Pyrite (Py), which is sparsely disseminated in skarns, with a small amount of biotite (Bt) and quartz (Qtz) generated along the cracks. It also contains muscovite (Ms) and biotite (Bt) in quartz and feldspars with pyrite (Py). Similarly, the Sample series (05-18) contains pyrite (Py) and molybdenite (Mol) associated visible quartz (Qtz), diopside (Dp), and calcite (Cl), with disseminated pyrite (Py). Additionally, Sample (07-4) contains pyrite (Py) and chalcopyrite (Cpy) with disseminated minerals, possibly including galena, sphalerite, or molybdenite (Mol). Likewise, Sample (07-13) shows visible disseminated mineralization, including quartz (Qtz), diopside (Dp), and pyrite (Py). The sample series (05-21) mainly contains quartz (Qtz) and epidote (Ep) skarn interbedded with garnet (Gt) and exhibits extremely weak mineralization. Meanwhile, Sample (05-6) contains minerals such as tremolite (Trm), muscovite (Ms), epidote (Ep), and garnet (Gt). Moreover, the sample series (01-7) contains muscovite, chlorite, diopside, and calcite, and the sample series (02-15) includes calcium iron garnet with visible ringed twin crystals and granular diopside.

Table 2. Sample numbers in each borehole and their petrographic descriptions.

| Borehole Number | S No | Petrographic Description |
|-----------------|-------|--|
| ZK8001 | 04-2 | Entirely of massive pyrite (Py) and molybdenite (Mol) associated with skarns. |
| | 05-1 | Pyrite (Py) is sparsely disseminated in skarn, a small amount of biotite (Bt), quartz (Qtz), muscovite (Ms), biotite (Bt) in quartz, and feldspars with pyrite (Py). |
| | 05-18 | Pyrite (Py) and molybdenite (Mol) are associated with visible quartz (Qtz), diopside (Dp), and calcite (Cl) with disseminated pyrite (Py). |
| CK3310 | 07-4 | Pyrite (Py), chalcopyrite (Cpy) with disseminated possibly galena, sphalerite, or molybdenite (Mol) association. |
| | 07-13 | Visible disseminated mineralization includes quartz (Qtz), diopside (Dp), and pyrite (Py). |
| CK338 | 5-21 | Quartz (Qtz) and epidote (Ep) skarn interbedded, containing garnet (Gt), with extremely weak mineralization. |
| | 05-6 | Tremolite (Trm), muscovite (Ms), epidote (Ep), and garnet (Gt). |
| | 01-7 | Muscovite, chlorite, diopside, and calcite. |
| | 02-15 | Calcium iron garnet, with visible ringed twin crystals, containing granular diopside. |

8. Conclusions

The research encompassed the implementation of a survey along a profile, denoted as profile-80. This profile served as the basis for acquiring the most optimal frequency of spread spectrum-induced polarization (SSIP) data. An intensive investigation was conducted in a complex research location, utilizing spread spectrum induced polarization (SSIP) data interpretation, geological analysis, and electrical parameter analysis of rock and ore samples from the Qiushawan mining area. This approach acquired valuable insights into the characteristics of conducting bodies C2, specifically molybdenum (Mo), and C4, specifically low-grade copper (Cu) and molybdenum (Mo) associated with skarn mineralization. By examining electrical properties and intricate geological characteristics, we successfully analyzed the SSIP data, enabling us to identify and describe these entities. Our work yielded resistivity models that played a crucial role in the identification of conductive entities. The models effectively depicted the spatial distribution of conductivity variations within the examined region. The accuracy of these models was verified by the drill results and overlaying geological sections onto both the resistivity and IP models. The alignment observed between the drilling data and the conductive entities in the resistivity models aided in authenticating and enhancing our confidence in the precision of the interpretations. The inclusion of geological sections, in conjunction with resistivity and IP models, facilitated the examination of potential correlations between geological characteristics and the observed conductivity variations within the models. The comparison bolstered our interpretations and augmented the value of our findings. The IP anomaly significantly influenced our research. By comparing IP anomalies with resistivity models and geological data, we successfully determined the presence of metallic minerals or changes in mineral composition. Through meticulous examination of these irregularities, we have obtained substantial knowledge regarding the potential mineral deposits and alterations in the composition of the study region. The resistivity models were verified by three drills and geological sections, as depicted in Figure 6. Following the SSIP survey, the drill verifications substantiated the existence of potential mineral resources in the studied area. Various minerals, including pyrite, molybdenite, chalcopyrite, epidote, calcite, and garnet, were found in the drilled core samples that were analyzed using petrography. Most of the samples frequently contained combined pyrite and molybdenite, while chalcopyrite, epidote, calcite, and garnet were rare accessory minerals. Large quantities of pyrite and molybdenite, found in conjunction with skarns, exclusively composed Sample (04-2). Sample (05-1) had a limited distribution of pyrite in skarns, accompanied by minor quantities of biotite and quartz formed along fissures. Sample (07-4) consisted of pyrite and chalcopyrite, along with scattered minerals that may be galena, sphalerite, or molybdenite. These findings offer useful insights for further investigation and assessment of the economic viability and scale of these mineral resources. Additional examination and investigation are required to assess the economic feasibility and determine the full magnitude of the mineral resources in the studied area. The findings of this study contribute to our understanding of the mineral potential and geological attributes of the Qiushawan Beishan copper–molybdenum deposit and the Qiushawan Nanshan skarn belt. The provided knowledge serves as a robust foundation for forthcoming exploratory endeavors and the promotion of sustainable resource development within the region. This will facilitate further research endeavors and contribute to informed decision-making about the governance of natural resources.

Author Contributions: J.A. conceptualized and designed the study, collected and analyzed the data, and wrote the manuscript. R.C. contributed to the study design and data analysis, critically revised the manuscript for important intellectual content, provided technical support and expertise in the data analysis, and contributed to the interpretation of the results. I.A., M.Y., S.F., O.A.R., F.U., S.A.S. and L.R. contributed to the data collection process. All authors have read and agreed to the published version of the manuscript.

Funding: This research was funded by the Basic Science Center Project of the National Natural Science Foundation of China, grant number 72088101.

Data Availability Statement: Data are contained within the article.

Acknowledgments: We would like to thank the Third Geological Brigade of Henan Nonferrous Geological Exploration Bureau for their help during the exploration process and for providing the final drilling verification results.

Conflicts of Interest: The authors declare no conflicts of interest.

References

1. Haldar, S.K. *Mineral Exploration: Principles and Applications*; Elsevier: Amsterdam, The Netherlands, 2018.
2. Kang, J.X.; Li, X.K. Thoughts on the development of molybdenum beneficiation technology. *IOP Conf. Ser. Earth Environ. Sci.* **2021**, *647*, 012001.
3. Long, J.; Zhang, S.; Luo, K. Discovery of anomalous molybdenum enrichment in ordovician and silurian stone coal: Relevance, origin and recommendations. *Chemosphere* **2023**, *320*, 137975. [[CrossRef](#)] [[PubMed](#)]
4. Michaux, S.P. *The Mining of Minerals and the Limits to Growth*; Geological Survey of Finland: Espoo, Finland, 2021.
5. Yang, Y.; Yang, Y.; Wu, G.; Li, J.; Chen, Y. Porphyry-skarn mo systems. In *Geology and Geochemistry of Molybdenum Deposits in the Qinling Orogen, PR China*; Springer: Singapore, 2022; pp. 363–516.
6. Zan, P.; Chen, S.; Chen, J.; Li, S. Early paleozoic adakitic granitoids from the xingshuping gold deposit of east qinling, china: Petrogenesis and tectonic significance. *Minerals* **2021**, *11*, 1032. [[CrossRef](#)]
7. He, J.; Xu, X.; Fu, Z.; An, Y.; Chen, T.; Xie, Q.; Chen, F. Decoupling of sr-nd isotopic composition induced by potassic alteration in the shapinggou porphyry mo deposit of the qinling–dabie orogenic belt, china. *Minerals* **2021**, *11*, 910. [[CrossRef](#)]
8. Gilder, S.; Courtillot, V. Timing of the north-south china collision from new middle to late mesozoic paleomagnetic data from the north china block. *J. Geophys. Res. Solid Earth* **1997**, *102*, 17713–17727. [[CrossRef](#)]
9. Liu, Q.; Li, H.; Shao, Y.; Girei, M.B.; Jiang, W.; Yuan, H.; Zhang, X. Age, genesis, and tectonic setting of the qiushawan cu–mo deposit in east qinling (central china): Constraints from sr–nd–hf isotopes, zircon u–pb and molybdenite re–os dating. *Ore Geol. Rev.* **2021**, *132*, 103998. [[CrossRef](#)]
10. Yan, D.-P.; Zhou, Y.; Qiu, L.; Wells, M.L.; Mu, H.; Xu, C.-G. The longmenshan tectonic complex and adjacent tectonic units in the eastern margin of the tibetan plateau: A review. *J. Asian Earth Sci.* **2018**, *164*, 33–57. [[CrossRef](#)]
11. Guo, B.; Zhang, Z.; Qin, Z. Geological characteristics and metallogeny of qiushawan porphyry type cu–mo deposit in east qinling. *Acta Geol. Sin. (Engl. Ed.)* **2014**, *88*, 1239–1240. [[CrossRef](#)]
12. Lu, X.; Yu, Z.; Feng, Y.; Wang, Y.; Ma, W.; Cui, H. Mineralization and tectonic setting of deep-hypabyssal granites in east qinling mountain. *Miner. Depos.* **2002**, *21*, 168–178.
13. Bao, Z.; Sun, W.; Zartman, R.E.; Yao, J.; Gao, X. Recycling of subducted upper continental crust: Constraints on the extensive molybdenum mineralization in the qinling–dabie orogen. *Ore Geol. Rev.* **2017**, *81*, 451–465. [[CrossRef](#)]
14. Mao, J.; Xie, G.; Bierlein, F.; Qü, W.; Du, A.; Ye, H.; Pirajno, F.; Li, H.M.; Guo, B.; Li, Y. Tectonic implications from re–os dating of mesozoic molybdenum deposits in the east qinling–dabie orogenic belt. *Geochim. Cosmochim. Acta* **2008**, *72*, 4607–4626. [[CrossRef](#)]
15. Bao, Z.; Xiong, M.; Li, Q. Petrogenesis of late mesozoic high-ba–sr granites in the qiushawan cumo orefield: Implications for the distribution of porphyry mo mineralization in the east qinling area of central china. *Lithos* **2019**, *348*, 105172. [[CrossRef](#)]
16. Sun, H.; Li, H.; Danišk, M.; Xia, Q.; Jiang, C.; Wu, P.; Yang, H.; Fan, Q.; Zhu, D. U–pb and re–os geochronology and geochemistry of the donggebi mo deposit, eastern tianshan, nw china: Insights into mineralization and tectonic setting. *Ore Geol. Rev.* **2017**, *86*, 584–599. [[CrossRef](#)]
17. Xie, Z.-J.; Xia, Y.; Cline, J.S.; Yan, B.-W.; Wang, Z.-P.; Tan, Q.-P.; Wei, D.-T. Comparison of the native antimony-bearing paiting gold deposit, guizhou province, china, with carlin-type gold deposits, nevada, USA. *Miner. Depos.* **2017**, *52*, 69–84. [[CrossRef](#)]
18. Zhang, Z.; Yang, X.; Dong, Y.; Zhu, B.; Chen, D. Molybdenum deposits in the eastern qinling, central china: Constraints on the geodynamics. *Int. Geol. Rev.* **2011**, *53*, 261–290. [[CrossRef](#)]
19. Mao, J.; Xie, G.; Pirajno, F.; Ye, H.; Wang, Y.; Li, Y.; Xiang, J.; Zhao, H. Late jurassic–early cretaceous granitoid magmatism in eastern qinling, central-eastern china: Shrimp zircon u–pb ages and tectonic implications. *Aust. J. Earth Sci.* **2010**, *57*, 51–78. [[CrossRef](#)]
20. Luo, B.; Zhang, H.; Zhang, L.; Zhang, C.; Shen, L.; Xiao, Z.; Pan, F.; Yang, H.; Li, Z.; Xu, W. The magma plumbing system of mesozoic shanyang porphyry groups, south qinling and implications for porphyry copper mineralization. *Earth Planet. Sci. Lett.* **2020**, *543*, 116346. [[CrossRef](#)]
21. Liu, W.; Chen, R.; Cai, H.; Luo, W.; Revil, A. Correlation analysis for spread-spectrum induced-polarization signal processing in electromagnetically noisy environments. *Geophysics* **2017**, *82*, E243–E256. [[CrossRef](#)]
22. Liu, W.; Chen, R.; Cai, H.; Luo, W. Robust statistical methods for impulse noise suppressing of spread spectrum induced polarization data, with application to a mine site, gansu province, china. *J. Appl. Geophys.* **2016**, *135*, 397–407. [[CrossRef](#)]
23. GSAI Geophysics. Electrical and Electromagnetic Instruments. 2019. Available online: <https://www.gs-ait.com/en/index.php/ProductCenter.html> (accessed on 7 August 2024).

Disclaimer/Publisher’s Note: The statements, opinions and data contained in all publications are solely those of the individual author(s) and contributor(s) and not of MDPI and/or the editor(s). MDPI and/or the editor(s) disclaim responsibility for any injury to people or property resulting from any ideas, methods, instructions or products referred to in the content.